Eleventh South African Conference on Computational and Applied Mechanics
SACAM 2018
Vanderbijlpark, South Africa, 17-19 September 2018

Improved accuracy considerations in Radial Basis Function surrogate models for variable resolution, scale, dimension and discontinuity

Gerhardus J Jansen van Rensburg[a], Alfred E J Bogaers[b]

[a,b] *Advanced Mathematical Modelling, Modelling and Digital Science, Council for Scientific and Industrial Research, Meiring Naudé Road, Brummeria, Pretoria 0185, South Africa*
[a,b] *Computer Science and Applied Mathematics, University of the Witwatersrand, Jan Smuts Avenue, Braamfontein Johannesburg 2000, South Africa*

email address : jjvrensburg@csir.co.za[a], abogaers@csir.co.za[b]

Abstract

Surrogate- or metamodels approximate and so reduce the computational cost associated with evaluating computer experiments of interest over a set of design variables. Radial Basis Functions (RBFs) are a popular metamodel choice due to its ease of implementation and availability in popular scientific programming languages. The correct use of RBF metamodels first require a model appropriate choice of basis function. The inclusion of a higher level model definition, using a polynomial for example, is another important consideration. By using cross-validation, dimensional scaling and error indicators calculated and inherited from Bayesian statistics or Machine Learning algorithms, the accuracy of the surrogate approximation can further be improved. Multiple surrogates may also be needed if discontinuities exist within the design space of the underlying computer experiment. In this conference contribution, many of these non-standard considerations are addressed and illustrated. The work focuses on the knowledge transfer and correct use of RBF surrogate models. The model implementation and considerations are first illustrated on benchmark test functions. This is followed by a CFD test-problem on the particular use of RBFs to construct a flight envelope of an object, illustrated using the interaction of two diamond airfoils. The test-problem shows the practical design of an RBF surrogate considering non-linearities in the drag, lift and moment coefficients as a result of interaction between various shock waves in the transonic and supersonic regime.

Keywords: Radial Basis Function; Surrogate Modelling; Flight Envelope

1. Introduction

Radial Basis Functions (RBFs) are used in a range of applications to approximate an underlying function or model by regressing or interpolating between values at a finite number of sample locations. RBF approximation is typically based on the sum of contributing bases using a simple multivariate neural network [1]. Interpolation using RBFs have been useful in reconstructing surface data from point clouds [2] and solving variational formulations to Partial Differential Equations [3]. It has also been used in mesh movement strategies [4] and interface information transfer [5] during Fluid Structure Interaction (FSI) simulations and non-linear registration [6]. RBF metamodels are further useful in reducing the cost of computationally expensive optimisation problems [7], sensitivity analyses [8] and simulation based complex engineering design [9].

To make effective use of RBF metamodels, it is important to consider the effects of multidimensional input data pre-processing, basis formulation and other choices made during fitting on the accuracy of the model constructed. This paper addresses some of these considerations applicable to the surrogate approximation of a field quantity sampled during the Design and Analysis of Computer Experiments (DACE) [10]. Section 2 of this paper focuses on knowledge transfer of the basics and the correct use of RBF approximates. This is presented using simple test functions to illustrate various important considerations that affect the efficacy of RBFs as a surrogate or metamodel approximation to a field quantity. In Section 3 a specific DACE approach and RBF metamodel to sampled Computational Fluid Dynamics (CFD) simulations is presented.

2. Radial Basis Functions

In this paper, radial basis functions are used to approximate a function $f(\boldsymbol{x})$ given f_i function values at discrete points $\boldsymbol{x_i}$. The approximation may be as a result of an interpolation or regression of the known function values in any number of input dimensions. The general surrogate model is constructed by treating the observed function values as if generated from the model

$$f_i = \sum_{k=1}^{M} \beta_k \phi(\boldsymbol{x}_i, \boldsymbol{x}_k) + p(\boldsymbol{x}_i) + \epsilon_i \qquad (1)$$

with β_k the weighting coefficient of the k^{th} basis function evaluation using the kernel or centre $\boldsymbol{x}_k$. The total basis function contribution results out of a summation of the contributions made by each basis function centre. The model may also have an underlying definition with $p(\boldsymbol{x})$ a polynomial and uncertainty captured by a normally distributed independent error term ϵ_i. In the case of exact interpolation, the error term is zero.

The basis functions $\phi(*)$ may take numerous functional forms. In this paper the $\boldsymbol{x}_k$ centre contribution is determined as a result of a Euclidean distance measure $r_k = \|\boldsymbol{x} - \boldsymbol{x}_k\|$, so that

$$\phi(\boldsymbol{x}_i, \boldsymbol{x}_k) = \phi(r_k). \qquad (2)$$

Some of the different functional forms possible that will be illustrated in this paper include:

- A second order poly-harmonic spline, commonly referred to as the Thin plate spline (TPS):
$$\phi(r) = r^2 \ln(\mathrm{r}). \qquad (3)$$
- A Gaussian function
$$\phi(r) = \exp[-(r/\varepsilon)^2\,]. \qquad (4)$$
with ε a tunable parameter associated with the radius of influence of a given or all basis function centres.
- The Inverse Multi-quadric function
$$\phi(r) = 1/\sqrt{1 + (r/\varepsilon)^2}. \qquad (5)$$
- A $\mathcal{C}^2$ continuous compact support function
$$\phi(r) = \begin{cases} (1 - r/\varepsilon)^4 (4r/\varepsilon\ + 1) & 0 \le r/\varepsilon \le 1 \\ 0 & r/\varepsilon > 1 \end{cases} \qquad (6)$$
here simply called CPC2.

2.1. Interpolation

As an illustrative example of how RBF interpolation is achieved, a one-dimensional test function

$$f(x) = \sin(8x) + 0.66\cos(18x) - 2x + 3; \quad 0 \leq x \leq 1, \tag{7}$$

is approximated using a list of sample locations $x_i \in \{0.0, 0.05, 0.15, 0.25, 0.4, 0.5, 0.6, 0.75, 0.9, 1.0\}$ resulting in the list of function values f_i. The test function is now approximated using interpolation with a second order polynomial and Gaussian functional form, effectively resulting in an approximation

$$S(x, \varepsilon) = \sum_{i=1}^{N} \beta_i \exp[-(|x - x_i|/\varepsilon)^2] + c_0 + c_1 x + c_2 x^2. \tag{8}$$

The weighting and polynomial coefficients can be determined by first constructing a correlation ($\boldsymbol{\Phi}$) and polynomial contribution ($\boldsymbol{P}$) matrix and then solving the system of equations expanded to

$$\begin{Bmatrix} f_1 \\ \vdots \\ f_n \\ 0 \\ 0 \\ 0 \end{Bmatrix} = \begin{bmatrix} \Phi_{11} & \cdots & \Phi_{1n} & 1 & x_1 & x_1^2 \\ \vdots & \ddots & \vdots & \vdots & \vdots & \vdots \\ \Phi_{n1} & \cdots & \Phi_{nn} & 1 & x_n & x_n^2 \\ 1 & \cdots & 1 & 0 & 0 & 0 \\ x_1 & \cdots & x_n & 0 & 0 & 0 \\ x_1^2 & \cdots & x_n^2 & 0 & 0 & 0 \end{bmatrix} \begin{Bmatrix} \beta_1 \\ \vdots \\ \beta_n \\ c_0 \\ c_1 \\ c_2 \end{Bmatrix}, \tag{9}$$

with $\Phi_{i,j} = \exp[-(|x - x_i|/\varepsilon)^2]$ using the Gaussian functional form of Eq. (4) and a choice of scalable radius of influence (ε). In Figure 1 the effect of different radii is illustrated with the red lines using coefficients as a result of the solution to the system of equations in (9) with (a) $\varepsilon = 0.01$, (b) $\varepsilon = 0.05$ and (c) $\varepsilon = 0.2$. In Figure 1(a), an underlying polynomial $p(x) = 4.13 - 8.49x + 6.42x^2$ is visible with small Gaussian "bumps" as a result of the highly localised radius of influence while (c) is the most accurate of the three when comparing the red and grey lines.

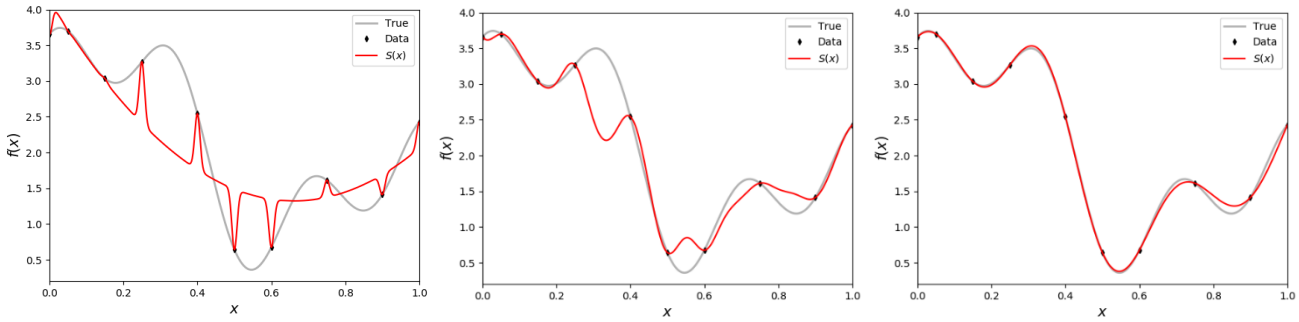

Figure 1: RBF approximations to the 1-D test function using Eq. (8) with (a) $\varepsilon = 0.01$, (b) $\varepsilon = 0.03$ and (c) $\varepsilon = 0.2$.

When tuning the scalable parameter(s), values that result in the best match to the true function is desired. The true function is however usually unknown or orders of magnitude more costly and time-consuming to evaluate - which is why the surrogate or metamodel is constructed in the first place. The scalable parameters are therefore usually fine-tuned by other means without comparison to a true function as discussed next.

2.2. Indicators

Supplementary indicators and uncertainty are further quantities that are very useful in fine-tuning the scalable parameters or developing an adaptive sampling strategy for example. The radius of influence or other scalable parameters may be fine-tuned without access to some "true" underling function by the use of cross-validation and maximising the likelihood function while uncertainty or prediction error indicators are useful in developing an adaptive sampling strategy.

2.2.1. Cross-validation

In the absence of a true known or easily determined function, the RBF approximation may be fine-tuned using cross-validation. The full set of data f_i is first split into a "training" and "testing" set or multiple sets if a lot of data is available. Given a set of tunable parameter values, a model is constructed using the training set(s) and the errors calculated between interpolated and true validation values in the testing set(s). If possible, a full "leave-one-out" cross validation is preferred. In this case N different models are constructed where each i^{th} model $S_i(\boldsymbol{x}, \boldsymbol{\varepsilon})$ is constructed without one sample value f_i at $\boldsymbol{x}_i$. The cross-validation objective function given a specific set of scalable parameter values $\boldsymbol{\varepsilon}$ is then

$$f_{\text{obj}}(\boldsymbol{\varepsilon}) = \sum_{i=1}^{N} \|S_i(\boldsymbol{x}, \boldsymbol{\varepsilon}) - f_i\|. \tag{10}$$

In Figure 2(a) the RBF approximation using all points but $x_4 = 0.25$ and $f_4 = 3.27$ using $\varepsilon = 0.1$ is illustrated. The blue line between the approximated and true sample value shows the particular contribution to total cross-validation error $\|S_4(0.25, 0.1) - 3.27\| = 0.868$. If all ten surrogate contributions are added the total cross-validation error according to Equation (10) is $f_{\text{obj}}(0.1) = 6.61$, corresponding to the function value of the black line in Figure 2(b) at a 0.1 radius of influence. For a very small and decreasing radius of influence, the objective function value seen in Figure 2(b) represents the difference between the underlying polynomial and each sample value so that $f_{\text{obj}} = 6.69$ while too large a support radius means samples are more correlated resulting in an increasingly ill-conditioned correlation matrix $\boldsymbol{\Phi}$. The minimum function value in Figure 2(b) is found at $\varepsilon = 0.262$ with $f_{\text{obj}}(0.262) = 1.789$. The corresponding approximation using Equation (8) with $\varepsilon = 0.262$ is given in Figure 2(c). This approximation results in an average error of 0.0202 or 1.429% when it and the true 1-D test function are compared using 1001 equispaced samples.

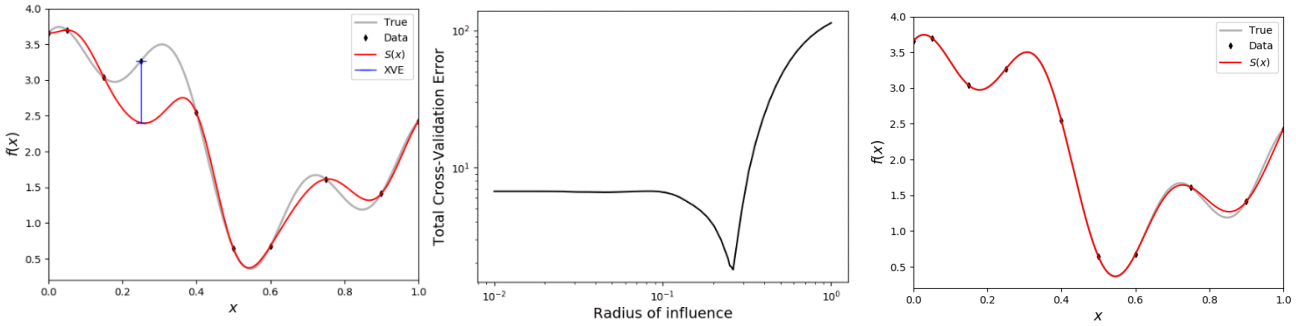

Figure 2: (a) $S_4(0.25, 0.1)$ in red with the cross-validation error in blue. (b) Total cross-validation error over a tested radius of influence $0.001 \leq \varepsilon \leq 1$ showing a strong minimum at $\varepsilon = 0.262$. (c) RBF approximation to the 1-D test function using Eq. (8) with $\varepsilon = 0.262$.

Full leave-one-out cross-validation are the ideal method for tuning scalable parameters, giving each sample point $N - 1$ chances to contribute to training and equal chance in testing the effect of parameters on the accuracy of the model. If there are large amounts of data or samples however, this process could in itself become too computationally expensive. An alternative would then be to split data into smaller groups of training and testing sets instead of using individual data points. A further alternative is to maximise the likelihood function as described next.

2.2.2. Likelihood

The RBF approximation in Eq. (1) is as a result of a set of correlated random variables indexed by the input space of $\boldsymbol{x}$. It is therefore possible to inherit useful characteristics from stochastic process models such as the concept of a likelihood function [7]:

$$\frac{1}{(2\pi)^{N/2}(\sigma^2)^{N/2}|\boldsymbol{\Phi}|} \exp\left[-\frac{(\boldsymbol{f} - \mathbb{1}\mu)^{\mathrm{T}}\boldsymbol{\Phi}^{-1}(\boldsymbol{f} - \mathbb{1}\mu)}{2\sigma^2}\right], \tag{11}$$

where $\boldsymbol{f}$ is the vector of the observed function values f_i and $\mathbb{1}$ is a vector of ones with the same length as the observations N. The scalable parameter dependence is captured via the correlation matrix $\boldsymbol{\Phi}$. For specific values of the scalable parameters, the mean μ and variance σ^2 values that maximize the likelihood function is

$$\hat{\mu} = \frac{\mathbb{1}^{\mathrm{T}}\boldsymbol{\Phi}^{-1}\boldsymbol{f}}{\mathbb{1}^{\mathrm{T}}\boldsymbol{\Phi}^{-1}\mathbb{1}} \quad \text{and} \quad \hat{\sigma}^2 = \frac{(\boldsymbol{f} - \mathbb{1}\hat{\mu})^{\mathrm{T}}\boldsymbol{\Phi}^{-1}(\boldsymbol{f} - \mathbb{1}\hat{\mu})}{N} \tag{12}$$

By substituting Equations (12) into the likelihood function, a concentrated likelihood function is produced as a function only scalable parameter values. The scalable parameter values that result in a maximum concentrated likelihood function value is an alternative to the fine-tuning discussed using the cross-validation process above. The logarithmic value of the likelihood function is explored for the same radius of influence range as in Figure 2(b) in Figure 3(a) for $0.01 \leq \varepsilon \leq 1$. The maximum of -10.84 is found as a result of $\varepsilon = 0.167$. This radius of influence results in an interpolation with an average error of 0.0364 or 2.397% seen in Figure 3(b).

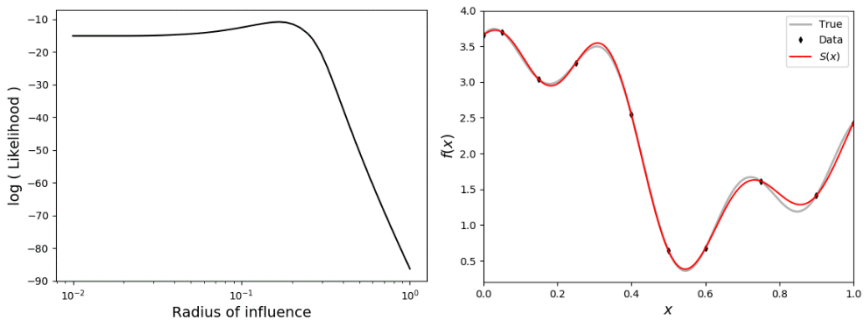

Figure 3: (a) Natural logarithm of the concentrated likelihood of the test function with (b) the RBF approximation corresponding to the radius of influence $\varepsilon = 0.167$ that maximises the likelihood function.

2.2.3. Estimated prediction error

The error made in interpolating between known sample locations at a specific location of interest $\boldsymbol{x}$ is estimated by first considering $\boldsymbol{\varphi}$ a vector containing the correlation $\phi(\boldsymbol{x}, \boldsymbol{x}_k)$ to all centre locations $\boldsymbol{x}_k$. Following the DACE approach [7], the mean squared error of the predicted interpolation value is estimated using

$$\varsigma^2(\boldsymbol{x}) = \sigma^2\left[1 - \boldsymbol{\varphi}^{\mathrm{T}}\boldsymbol{\Phi}^{-1}\boldsymbol{\varphi} + \frac{(1 - \mathbb{1}^{\mathrm{T}}\boldsymbol{\Phi}^{-1}\boldsymbol{\varphi})^2}{\mathbb{1}^{\mathrm{T}}\boldsymbol{\Phi}^{-1}\mathbb{1}}\right]. \tag{13}$$

The root mean squared error at a location of interest may be approximated by taking the square root of Equation (13). In Figure 4, the prediction error is estimated over the test-problem space using (a) $\varepsilon = 0.1$ (b) $\varepsilon = 0.167$ and (c) $\varepsilon = 0.1$. The square root is then used as a proxy for uncertainty in the form of an expected standard deviation from the prediction mean. The corresponding 95% confidence intervals are finally plotted as $S(\boldsymbol{x}) \pm 1.96\sqrt{\varsigma^2(\boldsymbol{x})}$.

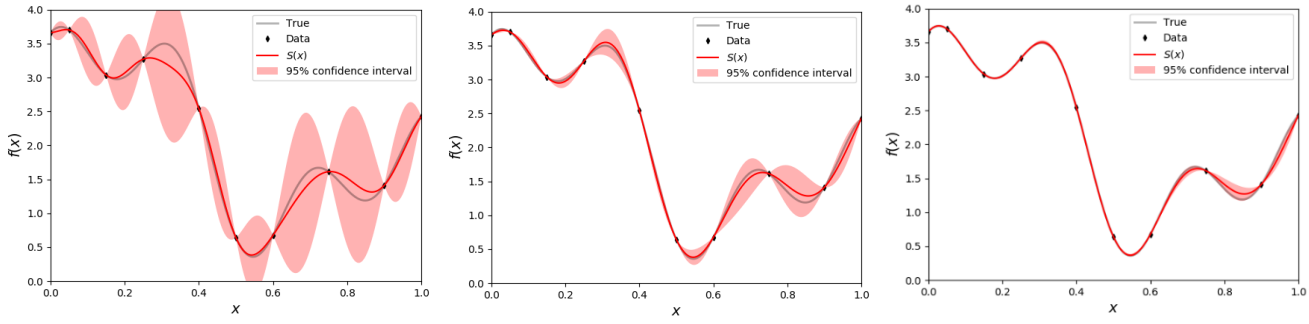

Figure 4: RBF approximation and $S(\boldsymbol{x}) \pm 1.96\sqrt{\varsigma^2(\boldsymbol{x})}$ using (a) $\varepsilon = 0.1$ (b) $\varepsilon = 0.167$ and (c) $\varepsilon = 0.1$.

2.3. Sharp discontinuities

If the function sampled and approximated has a sharp discontinuity, it is possible that an RBF interpolation results in an unusable surrogate. Points on either side of the discontinuity may be highly correlated using bases defined on the input space. This can be circumvented by adding a regularisation factor to the diagonal of the correlation matrix (i.e. $\Phi_{ii} + \lambda$) or regressing the data instead of solving it using the system of equations in Equation (9). This approach results in a continuous function approximation with less restriction on enforcing exact interpolation. As an example, Figure 5 shows approximations to a modified 1-D test function where any function value associated with $x > 0.6$ is recalculated using $f(x) + 1$. In Figure 5(a) no regularisation parameter is added meaning interpolation is exactly enforced between data values at $x = 0.6$ and $x = 0.60001$ resulting in an unusable approximation. A slight regularisation parameter however results in a useable surrogate approximation.

When confronted with a sharp discontinuity during metamodel approximations, it is best to model the problem using multiple approximations – each only affecting a region of interest. Using the useful approximation in Figure 5(c), the difference between known function value and interpolated values may be used as an indication of where to split regions of interest with one RBF surrogate for $0 \leq x \leq 0.6$ and another for $0.60001 \leq x \leq 1$. In higher input dimensions the presence of a sharp discontinuity or significantly finer model resolution will also be indicated by a significant deviation between interpolated and known sampled values. The discontinuity itself may then be modelled using another RBF regression known as Support Vector Machines [11] to classify which points and regions of input space belong to which region of interest.

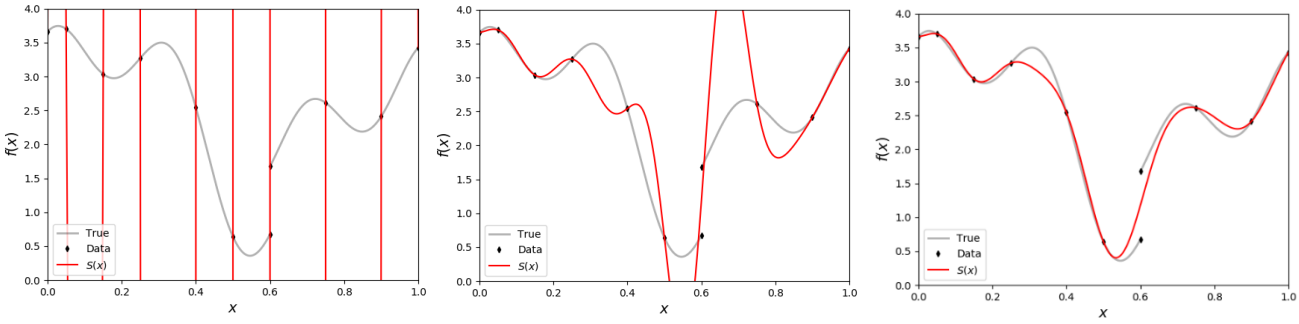

Figure 5: RBF interpolation in the presence of a sharp discontinuity using $\varepsilon = 0.1$ with Tikhonov regularisation parameter values (a) $\lambda = 0$, (b) $\lambda = 10^{-6}$ and (c) $\lambda = 10^{-5}$.

2.4. Regression

If there is a lot of noise in the sample values or a smoother function approximation is desired, it is possible to rather perform a least squares RBF regression instead of solving the interpolation equations in Equation (9). In this case the number of samples locations (now M) is likely larger than the number of RBF centres N. Written as $\boldsymbol{A} \times \boldsymbol{b} = \boldsymbol{f}$:

$$\begin{bmatrix} \Phi_{11} & \cdots & \Phi_{1n} & 1 & x_1 & x_1^2 \\ \vdots & \ddots & \vdots & \vdots & \vdots & \vdots \\ \Phi_{n1} & \cdots & \Phi_{nn} & 1 & x_n & x_n^2 \end{bmatrix} \begin{Bmatrix} \beta_1 \\ \vdots \\ \beta_n \\ c_0 \\ c_1 \\ c_2 \end{Bmatrix} = \begin{Bmatrix} f_1 \\ \vdots \\ f_n \end{Bmatrix}. \tag{14}$$

For a number of sample points more than the number of chosen RBF centres and number of polynomial coefficients (in the 1D test-function case $M > N + 3$), the coefficients are found as the least squares solution ($\boldsymbol{b}^*$) to the overdetermined system of equations in Eq. (14):

$$\boldsymbol{b}^* = (\boldsymbol{A}^{\mathrm{T}}\boldsymbol{A})^{-1}\boldsymbol{A}^{\mathrm{T}}\boldsymbol{f}. \tag{15}$$

In Figure 6 the result of this process using 500 points with a randomly assigned normally distributed error $\mathcal{N}(0,0.2)$ is illustrated using 11 equispaced kernels $x_i \in \{0.,0.1, 0.2, \ldots, 0.9, 1.0\}$. The change-off between local radii of influence and greater support is again visible when comparing Figure 6(a) to (c).

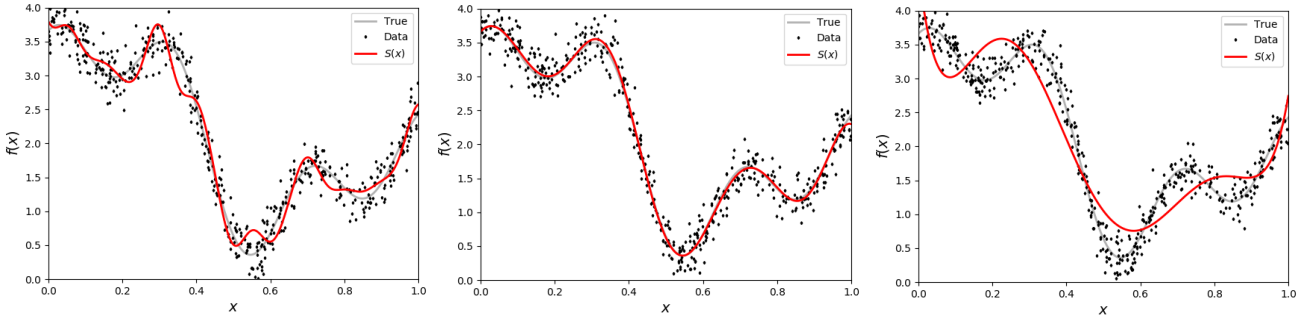

Figure 6: RBF regression using 11 equispaced centres and (a) $\varepsilon = 0.05$, (b) $\varepsilon = 0.2$ and (c) $\varepsilon = 2.0$

3. Aerodynamic test function

Surrogate models are very useful in a range of aerodynamic applications to interpolate or regress data obtained from wind tunnel experiments or CFD simulations. A complete flight envelope may be approximated using a well sampled variation in control parameters linked together using a surrogate model. In some cases, the data or underlying field of interest modelled may be a function of spatial position, angle of attack, Mach number, Reynolds number and control surface deflections. The surrogate-specific parameters can also be used to locally change the interpolation characteristics when special flow characteristics like shocks or flow separation are encountered.

In the work by Cleaver *et al.* [12], design of experiments and surrogate modelling techniques were used in a CFD environment to study forces and moments acting on a missile through various speeds and angles of attack. Rendall and Allen [13] used a multi-dimensional interpolation via radial basis functions to link experimental wind tunnel and computational surface pressure data through parameter space. Mackman *et al.* [14] illustrated a comparison of adaptive CFD sampling strategies to surrogate models of lift, drag and momentum coefficients (C_L, C_D and C_M) of a particular airfoil.

This test function considers a two diamond airfoil assembly, both at 0 degrees angle of attack. The airfoils have a chord length of 1 meter and a slope of 0.176. The airfoils are stacked with one translated 0.5m above the other. The horizontal distance between the centres is one of the input variables to the test function. The second variable is the velocity. CFD simulations are performed using a high speed aerodynamic solver called HiSA based on the OpenFOAM libraries [15]. As a detailed reference of the test function, 3264 different steady state CFD simulations were performed for 51 different horizontal distances from 0.5m to 1m and 64 different velocities between 100m/s and 700m/s. Figure 7 shows some results for pressure distribution at different velocity and distance between airfoils. Figure 7(a) shows the steady state solution with the second airfoil 0.65m behind the first at 305.2m/s while (b) is at 0.8m and 427.4m/s and (c) at 1m and 700m/s .

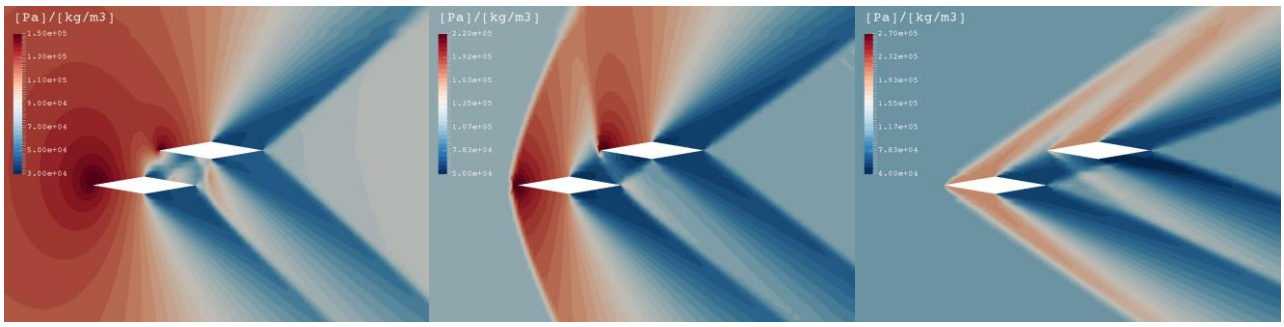

Figure 7: Simulated pressure contours (a) 0.65 at 305.2m/s (b) 0.8 at 427.4 (c) 1.0 at 700 m/s.

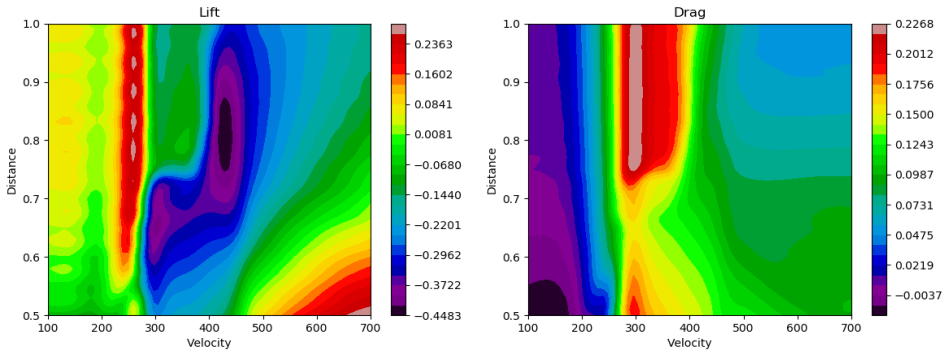

Figure 8: (a) Lift and (b) drag coefficients on the back airfoil as a result of different distances from the front and velocity.

The lift, drag and momentum coefficients for the second airfoil are extracted from the converged results. In Figure 8, contours of the lift coefficient (a) and drag coefficient (b) extracted from the 3264 total simulations are displayed.

Using the previously presented general insights into useful RBF surrogate attributes and accuracy considerations, this section further presents the construction of a DACE metamodel using some of the results of these CFD simulations as computer experiment samples. The lift coefficient contours in Figure 8(a) is used as the true values of the test-problem while a surrogate approximation is constructed using only 200 sample locations. This test case shows the practical design of an RBF surrogate considering non-linearities in the lift coefficient C_L as a result of interaction between various shock waves in the transonic and supersonic regime.

3.1. Naive surrogate

To start, the danger of a simple or naive surrogate approximation is illustrated. The test function is sampled at 200 locations determined by first constructing a 200 Latin Hypercube Design (LHD). The LHD used is displayed in Figure 9(a). Simply constructing a 2-D RBF surrogate using the sample input dimensions and lift coefficients results in the surrogate approximation illustrated in Figure 9(b). This illustrates the importance of scaling input dimensions. In this specific case a radius of influence $\varepsilon = 1$ means sample distance values between 0.5 and 1 will likely be correlated while the 200 sample velocities between 100 and 700 are highly uncorrelated unless they are sufficiently close. A simple way to overcome this issue is either allow variable scaling as a tuneable parameter or simply standardise input dimensions before constructing a surrogate approximation. Once input dimensions are standardised before surrogate approximation as in Figure 9(c), too large a radius of influence again results in an ill-conditioned correlation matrix and an over-fitted surrogate model.

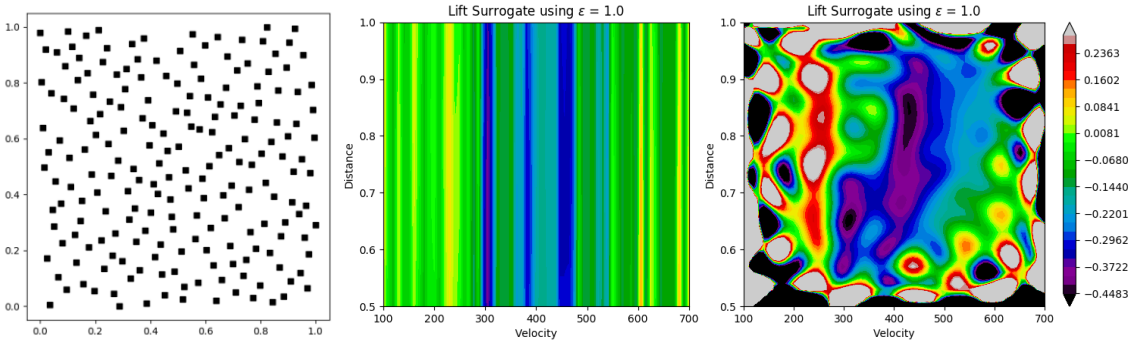

Figure 9: (a) 200 point 2-D Latin Hypercube Design. (b) Naive Gaussian RBF lift coefficient surrogate using unscaled input dimensions. (c) Over-fitted Gaussian RBF Lift surrogate.

3.2. Cross-validation

To tune and determine the best functional form out of Equations (3) to (6), the different forms are tested by comparing their cross-validation errors over a large radius of influence range using the standardised 200 LHD sample locations of Figure 9(a). The total "leave-one-out" cross validation as given in Equation (10) is compared for the Thin Plate Spline (TPS), Gaussian (GS), Inverse Multi-Quadric (IMQ) and $\mathcal{C}^2$ continuous compact support (CPC2) in Figure 10(a). The TPS has no scale effect with a total cross-validation error around 5.14 while a Gauss functional form using $\varepsilon = 0.3$ results in a total cross-validation error of 6.43. As a comparison, the over-fitted Gaussian lift surrogate in Figure 9(c) using $\varepsilon = 1.0$ has a total cross-validation error of 846.61. The best surrogate options according to the cross-validation study are either the use of an IMQ basis formulation using $\varepsilon = 0.3$ or the CPC2 functional form for a larger spread of radii between about 5 and 5000.

In Figure 10(b) the inverse multi-quadric approximation to the lift surrogate using $\varepsilon = 0.3$ is visible while (c) shows the CPC2 approximation using $\varepsilon = 1000$. The total 200 point cross-validation error of the IMQ surrogate using $\varepsilon = 0.3$ is 4.94 and the total error when all 3264 points are compared is 45.16. The CPC2 surrogate using $\varepsilon = 1000$ is 4.99 with a total error of 44.92.

If only 200 samples are considered possible, it would be better to perform non-uniform sampling based on areas of interest for an improved overall representation of the underlying lift coefficient as a function of distance and velocity. Considering work where more complex surrogates are desired as a function of many more parameters, an adaptive sampling strategy based on uncertainty and localised feature space is preferable. One such result is illustrated in the following subsection.

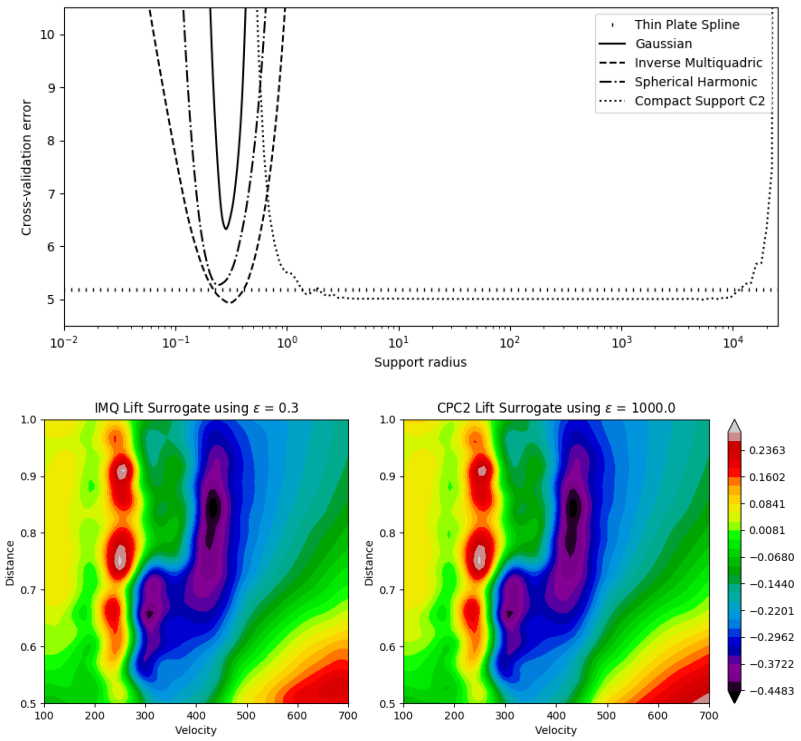

Figure 10: (a) Cross-validation error using different radius of influence (ε) and basis function formulation. (b) Inverse multi-quadric and (c) $\mathcal{C}^2$ piecewise continuous radial basis function interpolation approximates to the lift function in Figure 8(a) using the 200 point LHD.

3.3. Adaptive Sampling

One adaptive sampling strategy could be based on iteratively sampling the input space where the approximated variance or mean squared error using Equation (13) is a maximum [14]. This could be merely space-filling and does not fully take into account highly localised features. If on the other hand a highly localised feature is sub-sampled, the cross-validation error at that point could be high due to the smoothed surrogate approximation without taking that feature sample into account.

To take both uncertainty and localised cross-validation errors into account, an adaptive sampling strategy is presented that combines interpolated cross-validation error with approximated variance. The best combined function of these two indicators requires detailed consideration, but to merely illustrate this strategy using the lift coefficient test case, an initial LHD using 20 sample locations is set up and the 180 subsequent sample locations iteratively determined by maximising the selected sampling function

$$f_{\text{sample}}(\boldsymbol{x}) = \varsigma^2(\boldsymbol{x})[1000\, S_{\text{CVE}}(\boldsymbol{x}, \varepsilon)]^3 \tag{16}$$

with $\varsigma^2(\boldsymbol{x})$ defined in Equation (13) and $S_{\text{CVE}}(\boldsymbol{x}, \varepsilon)$ a surrogate approximating cross-validation errors instead of the original lift coefficient evaluated at the sample locations. A combination of variance and cross-validation error means the uncertain space closest to high cross-validation error locations is likely to be sampled. At each iteration, a new surrogate approximation is constructed and the next sample location similarly determined. The original 20 LHD and C_L approximation using $\varepsilon = 10$ is given in Figure 11(a). The cross-validation interpolation is given in Figure 11(b) and sampling function $f_{\text{sample}}(\boldsymbol{x})$ in (c). The final 200 points after additional adaptive sampling and corresponding lift coefficient approximation using $\varepsilon = 10$ is given in Figure 11(d). Here the non-uniform sampling strategy has produced dense sample locations in areas of local variation with sparse sampling in smoother areas. The cross-validation interpolation and sampling function using all 200 points are also given in Figure 11(e) and (f). The total cross-validation using these 200 sample locations and $\varepsilon = 10$ is 3.68 with a total error evaluated at all 3264 points of 23.36 meaning the lift coefficient is better approximated using this adaptive sampling strategy.

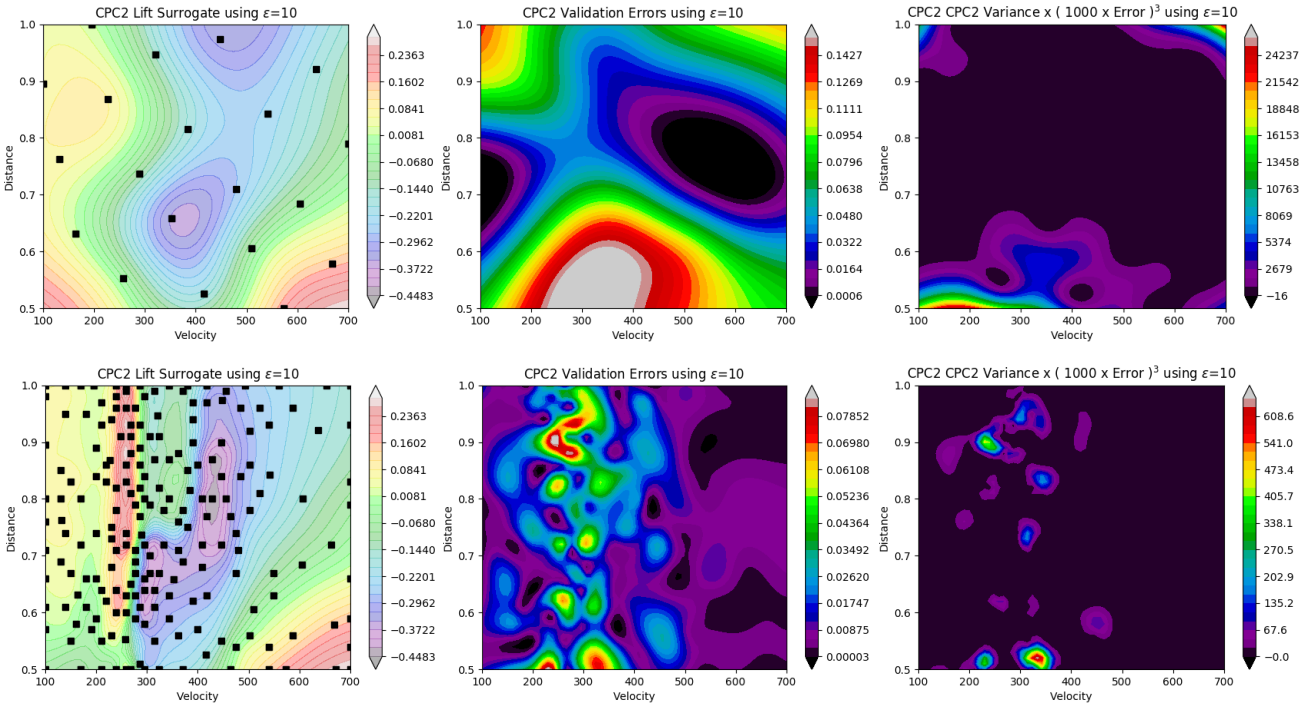

Figure 11: Adaptive sampling of the lift coefficient test function. (a) The original 20 point LHD and surrogate approximation with corresponding (b) cross-validation interpolation and (c) sampling function. The final 200 sample surrogate, validation error interpolation and sampling function are given in the bottom row (d-f).

4. Summary

This paper introduced and addressed some key aspects of radial basis function surrogate models. Useful supplementary indicators were illustrated to better scale tuneable parameters, estimate uncertainty and develop adaptive sampling strategies. The aerodynamic test case further addressed some of the considerations applicable to the DACE surrogate approximation of a field quantity. The test-problem shows the practical design of an RBF surrogate considering non-linearities in the lift coefficient as a result of interaction between various shock waves in the transonic and supersonic regime of a simple two diamond airfoil setup. The adaptive sampling approach presented may be used in constructing flight envelopes of more complex aerodynamic designs subject to higher variation in control or operating parameters or similar problems. This means a useful study or model could be developed at reduced computational cost than a full grid CFD simulation approach.

References

[1] Broomhead DH, Lowe D. (1988) Multivariable Functional Interpolation and Adaptive Networks. Complex Systems. 2:321-55.

[2] Carr JC, Beatson RK, Cherrie JB, Mitchell TJ, Fright WR, McCallum BC, Evans TR. (2001) Reconstruction and representation of 3D objects with radial basis functions. Proceedings of the 28th annual conference on Computer graphics and interactive techniques, ACM 67-76

[3] Wang JG, Liu G. (2002) A point interpolation meshless method based on radial basis functions. International Journal for Numerical Methods in Engineering. 54(11):1623-48.

[4] Bogaers AEJ, Kok S, Malan AG (2010) Highly efficient optimization mesh movement method based on proper orthogonal decomposition. International Journal for Numerical Methods in Engineering 86(8):935-52.

[5] Bogaers AEJ, Kok S, Reddy BD, Franz T. (2016) Interface information transfer between non-matching, nonconforming interfaces using radial basis function interpolation. Proceedings of the 10th South African Conference on Computational and Applied Mechanics (SACAM 2016), Potchefstroom, South Africa, 3-5 October 2016.

[6] Jansen van Rensburg GJ (2011) Selective feature preserved elastic surface registration in complex geometric morphology. Masters Dissertation, University of Pretoria.

[7] Jones DR, Schonlau M, Welch WJ (1998) Efficient global optimization of expensive black-box functions. Journal of Global Optimization 13:455-492.

[8] Jansen van Rensburg GJ, Kok S, Wilke DN (2014) Simultaneous boundary value and material parameter estimation using imperfect compression data. Proceedings of the 4th International Engineering Optimization Conference 2014 (EngOpt 2014), Instituto Superior Tecnico, Lisbon, Portugal, 8-11 September 2014.

[9] Liu H, Ong Y, Cai J (2018) A survey of adaptive sampling for global metamodeling in support of simulation-based complex engineering design. Journal of Structural and Multidisciplinary Optimization 57(1):395-416.

[10] Sacks J, Welch WJ, Mitchell TJ, Wynn HP (1989) Design and analysis of computer experiments (with discussion). Statistical Science 4:409-435.

[11] Smola AJ, Scholkopf B. (2004) A tutorial on support vector regression. Statistics and computing archive 14(3):199-222.

[12] Cleaver TA, Gutman AJ, Martin CL, Reeder MF, Hill RR (2016) Using design of experiments methods for applied computational fluid dynamics: A case study. Quality Engineering 28(3):280-292.

[13] Rendall TCS, Allen CB. (2008) Multi-dimensional aircraft pressure interpolation using radial basis functions. Proceedings of the Institution of Mechanical Engineers, Part G: Journal of Aerospace Engineering, 222:483-95.

[14] Mackman TJ, Allen BC, Ghoreyshi M, Badcock KJ (2013) Comparison of Adaptive Sampling Methods for Generation of Surrogate Aerodynamic Models. AIAA Journal 51(4):797-808.

[15] The OpenFOAM Foundation (2018) OpenFOAM v5 user guide. URL= https://cfd.direct/openfoam/user-guide